Supplementary Material

Magnetic resonance imaging- Human subjects

MRI was performed at the Soroka University Medical Center using a 3T Philips Ingenia scanner, and included: T1-weighted anatomical scan (3D gradient echo, TE/TR = 3.7/8.2 ms, acquisition matrix 432x432, voxel size: 0.5x0.5x1 mm), T2-weighted imaging (TE/TR = 90/3000 ms, voxel size 0.45x0.45x4 mm), FLAIR (TE/TR = 125/11000 ms, voxel size 0.5x0.5x4 mm), and susceptibility-weighted imaging (VenBOLD/ SWIp sequences, Philips). Diffusion tensor imaging (DTI) data were acquired using a single-shot echo-planar imaging (EPI) sequence with SENSE parallel imaging (reduction factor = 2.5, 33 directions with b = 1000 s/mm2, TE/TR = 106/9000 ms, axial slices parallel to the anterior-posterior commissure line, voxel size: 2.88×3.58x2 mm, 60 slices). For calculation of pre-contrast longitudinal relaxation times (T_{10}), variable flip angle (VFA) method was used (3D T1w-FFE, TE/TR = 2/10 ms, acquisition matrix: 256x256, voxel size: 0.89x0.89x6 mm, flip angles: 10,15,20,25 and 30°). Dynamic contrast-enhanced (DCE) sequence was then acquired (axial, 3D T1w-FFE, TE/TR = 2/4 ms, acquisition matrix: 192x187 (reconstructed to 256x256), voxel size: 0.9x0.9x6 mm, flip angle: 20°, Δt = 10 Sec, temporal repetitions: 100, total scan length: 16.7 min). An intravenous bolus injection of 0.1 mmol/kg of gadoterate meglumine (Gd-DOTA, Dotarem, Guerbet, France) was administered after the first five DCE repetitions using an automatic injector at a rate of 1.5 ml/sec.

Magnetic resonance imaging- Traumatic brain injury model

Mice were anesthetized with isoflurane (1.5%-2.5%) with respiration rate monitored throughout the procedure. Anatomical images were acquired using T1-weighted sequence (axial multi-slice multi-echo, TR/TE = 450/9 ms, in-plane resolution: 0.1 x 0.1 mm, slice thickness: 1 mm, acquisition matrix size: 220 x 220 px, 16 averages) and T2-weighted sequence (axial turbo spin echo RARE sequence, TR/TE = 3000/56 ms, in-plane resolution: 0.1 x 0.1 mm, slice thickness: 1 mm, acquisition matrix size: 220 x 220 px, 10 averages). DCE-MR images were acquired using T1-weighted gradient echo images (fast low angle shot sequence (FLASH)) with the following parameters: TR/TE = 102/1.9 ms, flip angle: 20^{o}, in-plane resolution: 0.17 x 0.17 mm, slice thickness: 1 mm, acquisition matrix size: 128 x 128 px, scan interval: 13 sec, 150 repetitions). During the dynamic sequence, 0.1 ml gadofosveset trisodium (Ablavar, 0.25 mmol/ml, Lantheus Medical Imaging Inc., North Billerica, MA)

was administered by intravenous tail vein injection after 5 baseline scans. Then, 145 scans were acquired over 31 min. Tissue harvesting was performed 1.5 hours after the last scan. Mice were sacrificed via CO_2 narcosis and transcardially perfused with phosphate-buffered saline. For gross pathology assessment, brains were imaged using Nikon D5200 digital camera. Ultra-trace elemental and isotopic analytical brain mapping for gadolinium (157Gd) and phosphorus (31P) was performed by laser ablation-assisted MIMS at the Boston University Center for Biometallomics (CBM) as reported (Craddock *et al.*, 2012; Tagge *et al.*, 2018).

Vascular injury model

Briefly, under deep anesthesia (intraperitoneal ketamine and xylazine 100 mg/ml, 0.08 ml/100 gr and 20 mg/ml, 0.06 ml/100 gr, respectively), the tail vein was catheterized. Body temperature was continuously monitored and maintained at 37 ± 0.5^{o}C using a feedback-controlled heating pad (Physitemp Ltd.). Heart rate, breath rate and oxygen saturation levels were continuously monitored (STARR, Life Sciences Ltd.). Imaging was performed using the open window method. A 1x1 mm^2 cranial section was removed over the right sensory-motor cortex (1 mm caudal, 3 mm lateral to bregma) and the subjacent cortical section was exposed by removing the dura and arachnoid layers. This section was continuously perfused with artificial cerebrospinal fluid (ACSF) containing (in mM): 124 NaCl, 26 $NaHCO_3$, 1.25 NaH_2PO_4, 2 $MgSO_4$, 2 $CaCl_2$, 3 KCl, and 10 glucose (pH 7.4).

For thrombolytic stroke induction, the photo-reactive substance Rose bengal (RB, 7.5 mg/ml, 0.133 ml/100 g, in 0.9% NaCl) was injected into the tail vein, while a vascular region in the cortex was laser-illuminated for 15 min at 660 nm (Cellvizio, Mauna Kea Technologies). The bone window was covered with bone cement and bone-wax. Rat was sutured and put back in cage for recovery. Twenty-four hours post-photothrombosis, the rat was re-anesthetized and a cranial section around the bone window was removed (4 mm caudal, 5 mm lateral, 1 mm frontal to bregma). The open window was continuously perfused with ACSF.

Intravital fluorescence imaging was performed 24 hours after injury using a fluorescence microscope (Zeiss SteREO Lumar V12; Oberkochen, Germany). Images were captured at x30-40 magnification. The non-BBB permeable fluorescent dye NaFlu was injected intravenously (1 mg/ml, 0.2 ml/injection, in 0.9% NaCl). Full-resolution (658×496 pixels) images of cortical surface vessels were acquired (1 frames/second, EMCCD camera: Andor Technology, DL-658 M-TIL) before, during and after injection of the tracer, for 30 min.

For MRI, rats were anesthetized using ketamine (100 mg/ml, 0.08 ml/100 gr) and xylazine (20 mg/ml, 0.06 ml/100 gr) and body temperature was continuously monitored as described above. As previously described (Lippmann *et al.*, 2017), to induce photothrombosis the calvarium was exposed to a light beam that was vertically centered 1 mm posterior and 1 mm lateral from bregma. Rose bengal was administered intravenously (7.5 mg/ml, 0.133 ml/100 g, in 0.9% NaCl) and a halogen light beam (diameter 3.5 mm) was directed for 15 min onto the intact skull. Following the procedure, the rat was sutured and put back in cage for recovery. MRI, including anatomical and DCE-MRI, was performed 24 hours after injury under isoflurane anesthesia using a pre-clinical system (Aspect Imaging, M2 high performance MRI, Shoham, Israel) as reported (Lippmann *et al.*, 2017). T2-w images were obtained using fast spin echo sequences (TR/TE/NEX = 3400/74/4). T1w spin echo classic scans (TR/TE/NEX = 400/14/2) were acquired before (one scan) and after (nine scans) intravenous injection of gadoterate meglumine (Gd-DTPA, 0.5M, 1 ml/Kg, Dotarem, Soreq Radiopharmacieuticals Ltd.).

Recurrent seizure model

Recurrent seizures were induced by perfusion of the cortical surface with 4-aminopyridine (4-AP; 500 μM) in ACSF. Electrocorticogram (ECoG) was recorded using bipolar electrodes and a telemetric recording system (Data System International). Probe-based confocal laser microscopy (PCLM) was performed using Cellvizio dual band (Mauna Kea Technologies) at 488 and 660 nm and analyzed with in-house developed MATLAB (Mathworks, Natick, MA) scripts.

Animal BBB permeability analysis by intravital fluorescence imaging

Probe-based confocal laser microscopy (PCLM) images were obtained to quantify the diffusion of EB-albumin complex during prolonged seizures (Vazana *et al.*, 2016). Full resolution cortical images (576x574) were acquired and resized (128x128). A third compartment indicating a vessel wall region was manually selected and its nearby luminal area was selected from the vascular region (vessel lumen).

Signal intensity changes over time and space were then analyzed and signal histograms were calculated for each 5 min sequence for vessel lumen, vessel wall and extravascular space. The histogram indicates the dependency between fluorescence intensity and its probability of appearance in the dynamic sequence. Signal intensity with the highest probability is the

dominant signal level in the analyzed sequence. Evaluation of EB-albumin transfer from vessel lumen to vessel wall and from vessel lumen to extravascular space was done by calculating the difference in area under curve (AUC) between compartments. For example, the permeability from the lumen to the wall is: $\frac{AUC^{wall}-AUC^{lumen}}{|AUC^{lumen}|}$; positive values indicate transfer from vessel lumen to wall/extravascular space. Permeability levels were normalized to those calculated while the exposed cortex was perfused with ACSF alone (control).

Ex vivo assessment of BBB permeability in rat

Under deep anesthesia (isoflurane, 2-3%), Evan blue was injected to the tail vein (n = 4, 48 mg/kg). After 30 min, rats were intracardially perfused with phosphate-buffered saline (PBS) containing 4% paraformaldehyde (PFA). For immunohistochemistry, brains were cryoprotected with sucrose gradient (10% followed by 20 and 30% sucrose in PBS) and 30 µm-thick coronal sections were obtained using a freezing microtome (Leica Biosystems). Immunofluorescence was performed in the free-floating sections with primary anti-GFAP antibody (Dako Z0334), followed by secondary antibody donkey anti-rabbit IgG-Alexa Fluor 488 (ThermoFisher Scientific, A21206), both diluted 1:500. Sections were visualized with Zeiss Axioplan 2.

Diffusion tensor imaging analysis

Analysis was performed on 17 controls and 25 players that were scanned only during the season. Identification of the anterior commissure (AC), posterior commissure (PC) and mid-sagittal plane was performed manually and a rigid transform was used for the rotation of the T1-weighted images to AC–PC aligned space. Following correction for head movements and eddy-current distortions, a nonlinear constrained transformation (Rohde *et al.*, 2004) was used to register the diffusion data to the non-diffusion weighted image (b0). Registration of b0 to T1 anatomy images was performed using mutual information maximization methods implemented in SPM8. Finally, a tensor model, fit to the data in each voxel, was applied using a robust least-squares algorithm that removed outliers during tensor estimation (Robust Estimation of Tensors by Outlier Rejection, RESTORE (Chang *et al.*, 2005)). This yielded three diffusion eigenvectors and eigenvalues of the tensor, based on which the diffusion parameters including FA, MD, RD and AD, were calculated for 20 tracts of each scan. For selected fibers, the FFDD method (Benou *et al.*, 2019) was used. The method combines geometric properties of fiber bundles with local scalar diffusion measurements (e.g. FA) into

a single descriptor, enabling a sensitive tract-wise analysis that also includes structural variations. FFDD is calculated by combining changes in the geometric properties of selected bundle of fibers with diffusivity measurements (e.g. MD, FA, RD or AD). The result is a vector of values of the diffusion parameter along a tract, whose values also represent changes in the fiber's geometry.

Supplementary Table S1. Comparison of the characteristics of players with or without signs of BBBD. Symptoms score and standardized assessment of concussion were calculated using the NFL sideline concussion assessment tool (2013).

	Normal players (*n*= 32) median (25%-75%, min-max)	**Abnormal players (*n*= 9) median (25%-75%, min-max)**	***p*-value (Mann-Whitney *U*-test)**
Age	25 (23.25-26.75, 18-39)	29 (27-31, 20-32)	**0.028***
Years playing	3 (2-6, 1-20)	2.5 (1-5.5, 1-6)	0.375
Age at start	21.5 (19.25-23, 14-32)	25 (23-28.5, 19-31)	**0.008****
Concussion #	1 (0-2, 0-6+)	0 (0-2.5, 0-6+)	0.633
Symptoms #	2 (1-5.5, 0-17)	1.5 (0.5-4, 0-6)	0.42
Symptoms score	3 (1-8, 0-25.5)	3.5 (0.5-9.5, 0-16)	0.94
Standardized Assessment of Concussion (SAC)	27 (26-28.5, 22.5-30)	26.5 (24.875-28.5, 23.5-30)	0.55

Supplementary Table S2. Reported concussion history and subsequent symptoms among study participants.

Concussions	Players, # (%)	Symptoms (# of reports)	Controls, # (%)	Symptoms (# of reports)
0	19 (46.3 %)		20 (74%)	
1	9 (21.9 %)	Blackout (3), dizziness (2), blurred vision (2), headache (2), head ringing (1), temporary amnesia (1), nausea (1)	4 (14.8%)	Headache (1), Loss of consciousness (1), blackout (1), confusion (1)
2	6 (14.6 %)	Dizziness (3), headache (2), vomiting (2), blurred vision (1), visual color distortion (1), balance problems (1), neck pain (1), confusion (1), blackout (1)	1 (3.7%)	Dizziness
3	2 (4.9 %)	Headache (2), neck pain (1), dizziness (1), blurry vision (1), nausea (1)	0	
4	1 (2.4 %)	Headache, neck pain, confusion, difficulty concentrating for a couple of days	0	
5	0 (0)		0	
6+	4 (9.8 %)	Blurred vision (3), balance problems (2), headache (2), neck pain (2), dizziness (1), problems focusing (1)	2 (7.4 %)	Headaches (2), dizziness (2), vomiting (1)

Supplementary Table S3. Diffusion parameters of white matter tracts that were significantly different between American football players and controls.

Diffusion parameter	Fiber name	Valid controls	Valid players	Mann-Whitney *U*-test Z score	*p*-value
FA	Left thalamic radiation	16	23	2.48	0.01
	Corpus callosum forceps minor	17	25	2.57	0.01
	Left inferior fronto-occipital fasciculus (IFOF)	14	10	2.91	0.003
	Left inferior longitudinal fasciculus (ILF)	16	23	3.79	<0.001
MD	Right arcuate	14	21	2.05	0.03
RD	Corpus callosum forceps minor	17	25	-2.13	0.03
	Left inferior fronto-occipital fasciculus (IFOF)	13	10	-2.54	0.01
	Right inferior longitudinal fasciculus (ILF)	16	23	-3.05	0.002
AD	Left cortico-spinal	17	25	2.42	0.01
	Right cortico-spinal	17	26	2.26	0.02
	Corpus callosum forceps major	11	14	2.57	0.01

Supplementary Fig. 1. Regional analysis of BBBD in American-football players. BBBD maps are shown for brains of controls (left) and players (right). Each brain scan was registered and segmented into 126 anatomically defined regions according to the MNI brain atlas (see Methods). The percentage of voxels with high BBB permeability (contrast accumulation rates exceeding the intensity threshold) was quantified within each region and BBBD was defined if the percentage of voxels was >2 SDVs from the mean percentage in healthy controls. Color codes for the percentage of individuals with BBBD in each region.

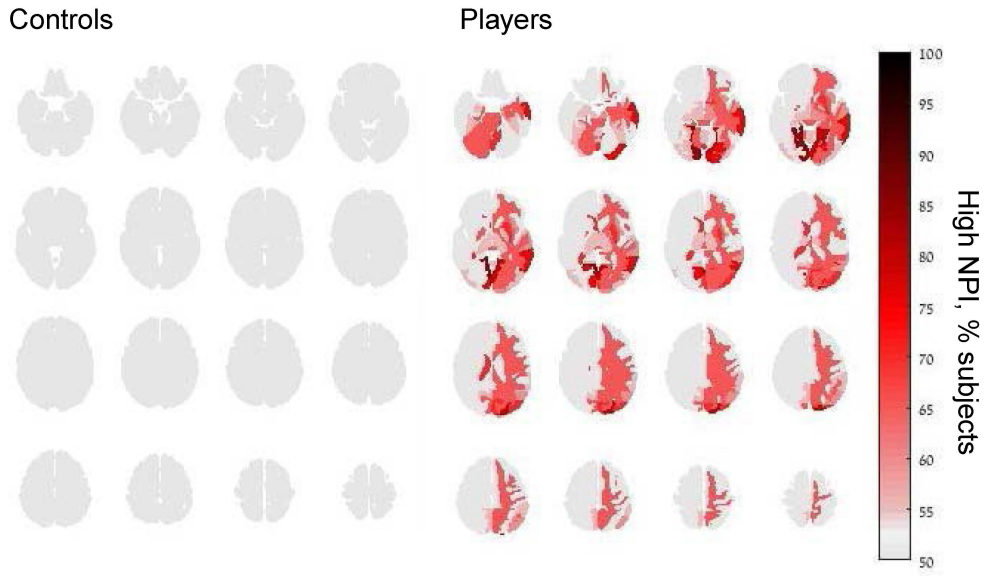

Supplementary Fig. 1. Regional analysis of BBBD in American-football players

Supplementary Fig. 2. Tofts analysis in American-football players. K^{trans} values were calculated for each brain voxels in healthy controls and players. Similar to the calculation of NPI values (see Methods and Fig. 1G) a threshold was set to define abnormally high K^{trans} values (95^{th} percentile of controls) and the percentage of brain voxels with high K^{trans} were plotted for the entire brain volume ("whole brain"), gray and white matter. No differences found between players and controls.

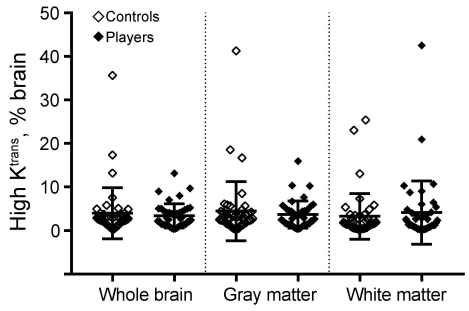

Supplementary Fig. 2. Tofts analysis in American-football players

Supplementary Fig. 3. Slow brain accumulation of contrast agent in a DCE-MRI from an amateur American-football player. Representative NPI map from a player (**A**). Signal enhancement curve reveal pattern of a slow accumulation of contrast agent that is clearly observed starting several minutes after injection of the contrast-agent, in the left hemisphere (**B, red line**). The normal pattern of contrast washout is observed in the superior sagittal sinus and right occipital brain region (blue and green lines, respectively). A linear fit of the late part of the curve (dashed line) was used to calculate values for the slow BBB leak. Normalized permeability (NPI) was calculated for comparison between individuals (e.g. healthy controls) by dividing the slope calculated for each voxel to that of the super sagittal sinus from the same individual.

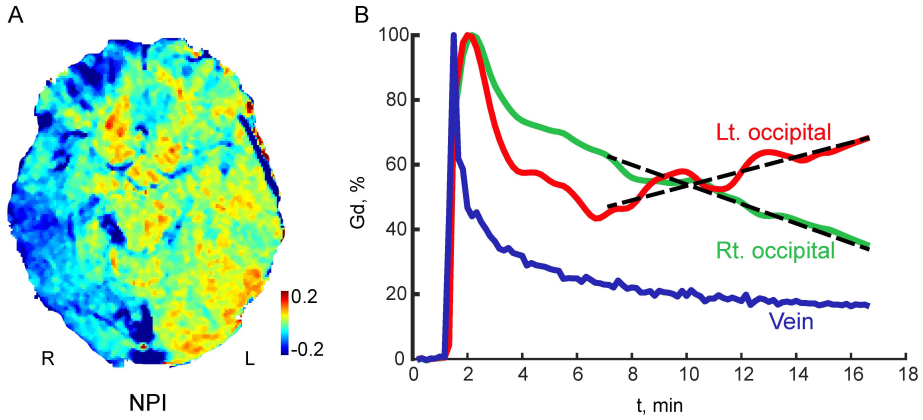

Supplementary Fig. 3. Slow brain accumulation of contrast agent in a DCE-MRI from an amateur American-football player

Supplementary references:

Supplementary references:

Benou I, Veksler R, Friedman A, Raviv TR. Combining white matter diffusion and geometry for tract-specific alignment and variability analysis. Neuroimage 2019; 200: 674–689.

Chang LC, Jones DK, Pierpaoli C. RESTORE: Robust estimation of tensors by outlier rejection. Magn Reson Med 2005; 53: 1088–1095.

Craddock TJA, Tuszynski JA, Chopra D, Casey N, Goldstein LE, Hameroff SR, et al. The zinc dyshomeostasis hypothesis of Alzheimer's disease. PLoS One 2012; 7: e33552.

Lippmann K, Kamintsky L, Kim SY, Lublinsky S, Prager O, Nichtweiss JF, et al. Epileptiform activity and spreading depolarization in the blood–brain barrier-disrupted peri-infarct hippocampus are associated with impaired GABAergic inhibition and synaptic plasticity. J Cereb Blood Flow Metab 2017; 37: 1803–1819.

Rohde GK, Barnett AS, Basser PJ, Marenco S, Pierpaoli C. Comprehensive Approach for Correction of Motion and Distortion in Diffusion-Weighted MRI. Magn Reson Med 2004; 51: 103–114.

Tagge CA, Fisher AM, Minaeva O V., Gaudreau-Balderrama A, Moncaster JA, Zhang XL, et al. Concussion, microvascular injury, and early tauopathy in young athletes after impact head injury and an impact concussion mouse model. Brain 2018; 141: 422–458.

Vazana U, Veksler R, Pell GS, Prager O, Fassler M, Chassidim Y, et al. Glutamate-Mediated Blood–Brain Barrier Opening: Implications for Neuroprotection and Drug Delivery. J Neurosci 2016; 36: 7727–7739.